CHAPTER 23
METEOROLOGICAL RADAR

Robert J. Serafin
*National Center for Atmospheric Research**

23.1 INTRODUCTION

As this handbook is being written, dramatic changes are taking place in the field of radar meteorology. While the majority of radar engineers are familiar with current operational meteorological radars, few are aware of the advances that have been made in the past two decades. For example, doppler radar meteorology, using modern digital signal-processing techniques and display technology, has moved ahead so rapidly that the United States is now planning to replace its existing operational weather radar network with a next-generation doppler system (NEXRAD). This system will provide quantitative and automated real-time information on storms, precipitation, hurricanes, tornadoes, and a host of other important weather phenomena, with higher spatial and temporal resolution than ever before.[1] A second network of doppler radars, in airport terminal areas, will provide quantitative measurements of gust fronts, wind shear, microbursts, and other weather hazards for improving the safety of operations at major airports in the United States.[1,2] Next-generation doppler radars that use flat-plate antennas, color displays, and solid-state transmitters are now available for commercial aircraft. And many of these new technologies are being deployed in countries throughout the world.

In the research arenas, multiple-doppler radars are used for deriving three-dimensional wind fields.[3] Airborne doppler radar[4,5] has been used to duplicate these capabilities, thus providing for great mobility. Polarization diversity techniques[6] are used for discriminating ice particles from water, for improved quantitative precipitation measurement, and for detecting hail. And there is a new family of radars, ultrahigh-frequency (UHF) and very-high-frequency (VHF) fixed-beam systems that are being used to obtain continuous profiles of horizontal winds.[7] These examples are illustrative of the vitality of the field.

This chapter is intended to introduce the reader to meteorological radar and particularly those system characteristics that are unique to meteorological applications. In this regard, it should be noted that most meteorological radars appear

*The National Center for Atmospheric Research is sponsored by the National Science Foundation.
Special thanks are due to Victoria Holzhauer for her careful typing, assistance with figures, and editing of this manuscript. The author is also grateful to Richard Carbone and Jeffrey Keeler for their critical reviews.

similar to radars used for other purposes. Pulsed and pulsed doppler systems are common. Parabolic dish antennas, focal-point feeds, and low-noise solid-state receivers are used. Magnetrons, phase-locked magnetrons, klystrons, traveling-wave tubes, and other forms of transmitters are used.

The major distinction between meteorological radar and other kinds of radars lies in the nature of the targets. Meteorological targets are distributed in space and occupy a large fraction of the spatial resolution cells observed by the radar. Moreover, it is necessary to make quantitative measurements of the received signal's characteristics in order to estimate such parameters as precipitation rate, precipitation type, air motion, turbulence, and wind shear. In addition, because so many radar resolution cells contain useful information, meteorological radars require high-data-rate recording systems and effective means for real-time display.[8,9] Thus, while many radar applications call for discrimination of a relatively few targets from a clutter background, meteorological radars focus on making accurate estimates of the nature of the *weather clutter* itself. This poses some challenging problems for the radar system designer to address.

The discussion here will refer to a number of useful texts and references for the reader to use. However, Battan's text,[10] revised in 1973, deserves special mention for its clarity and completeness and remains a standard for courses in radar meteorology that are taught in universities around the world. Doviak and Zrnić[11] place special emphasis on doppler meteorological radar. Chapter 24 in the first "Radar Handbook," by Bean et al.,[12] addresses the problem of weather effects on radar. Finally, perhaps the broadest and most complete set of references on progress in the field can be found in the *Proceedings* and *Preprints* of the series of radar meteorology conferences sponsored by the American Meteorological Society (AMS). These documents can be found in most technical libraries and also can be obtained through the offices of the AMS in Boston.

23.2 THE RADAR RANGE EQUATION FOR METEOROLOGICAL TARGETS

The received power from distributed targets can be derived from any of a variety of expressions that are applicable to radar in general. A simple form, with which to begin, is given below:

$$P_r = \frac{\beta\sigma}{r^4} \tag{23.1}$$

where β is a constant dependent upon radar system parameters, r is the range, and σ is the radar cross section.

It is in the calculation of σ for meteorological targets that the radar range equation differs from that for point targets. σ may be written

$$\sigma = \eta V \tag{23.2}$$

where η is the radar reflectivity in units of cross-sectional area per unit volume and V is the volume sampled by the radar. η can be written as

$$\eta = \sum_{i=1}^{N} \sigma_i \tag{23.3}$$

where N is the number of scatterers per unit volume and σ_i is the backscattering cross section of the ith scatterer. In general, the meteorological scatterers can take on a variety of forms, which include water droplets, ice crystals, hail, snow, and mixtures of the above.

Mie[13] developed a general theory for the energy backscattered by a plane wave impinging on spherical drops. This backscattered energy is a function of the wavelength, the complex index of refraction of the particle, and the ratio $2\pi\alpha/\lambda$, where α is the radius of the spherical particle and λ is the wavelength.

When the ratio $2\pi\alpha/\lambda \ll 1$, the Rayleigh approximation[10] may be applied, and σ_i becomes

$$\sigma_i = \frac{\pi^5}{\lambda^4}|K|^2 D_i^6 \tag{23.4}$$

where D_i is the diameter of the ith drop and

$$|K|^2 = \left|\frac{m^2 - 1}{m^2 + 2}\right|^2 \tag{23.5}$$

where m is the complex index of refraction. At temperatures between 0 and 20°C, for the water phase, and at centimeter wavelengths

$$|K|^2 \approx 0.93 \tag{23.6a}$$

and for the ice phase

$$|K|^2 \approx 0.20 \tag{23.6b}$$

Equation (23.3) can now be written as

$$\eta = \frac{\pi^5}{\lambda^4}|K|^2 \sum_{i=1}^{N} D_i^6 \tag{23.7}$$

and the radar reflectivity factor Z defined as

$$Z \sum_{i=1}^{N} D_i^6 \tag{23.8}$$

In radar meteorology, it is common to use the dimensions of millimeters for drop diameters D_i and to consider the summation to take place over a unit volume of size 1 m^3. Therefore, the conventional unit of Z is in mm^6/m^3. For ice particles, D_i is given by the diameter of the water droplet that would result if the ice particle were to melt completely.

It is often convenient to treat the drop or particle size distribution as a continuous function with a number density $N(D)$, where $N(D)$ is the number of drops per unit volume, with diameters between D and $D + dD$. In this case, Z is given by the sixth moment of the particle size distribution,

$$Z = \int_0^\infty N(D) D^6 dD \tag{23.9}$$

If the radar beam is filled with scatterers, the sample volume V is given[10] approximately by

$$V \approx \frac{\pi\theta\phi r^2 c\tau}{8} \tag{23.10}$$

where θ and ϕ are the azimuth and elevation beamwidths, c is the velocity of light, and τ is the radar pulsewidth.

Substituting Eqs. (23.10), (23.2), and (23.4) into Eq. (23.1) gives

$$\begin{aligned} P_r &= \frac{\beta\pi}{r^4}\frac{\theta\phi r^2 c\tau}{8}\frac{\pi^5}{\lambda^4}|K|^2\sum_{i=1}^{N} D_i^6 \\ &= \frac{\beta\pi^6\theta\phi\, c\tau\, |K|^2}{8\lambda^4 r^2} Z \\ &= \frac{\beta' Z}{r^2} \end{aligned} \tag{23.11}$$

This simple expression illustrates that the received power is a function only of β' (a constant dependent upon radar system parameters), is proportional to the radar reflectivity factor Z, and is inversely proportional to r^2.

In actual fact, the antenna gain is not uniform over the beamwidth, and the assumption of a uniform gain can lead to errors in the calculation of Z. Probert-Jones[14] took this into account, assumed a gaussian shape for the antenna beam, and derived the following equation for the received power:

$$P_r = \frac{P_t G^2 \lambda^2 \theta\phi\, c\tau}{512(2 \ln 2)\pi^2 r^2} \sum_{i=1}^{N} \sigma_i \tag{23.12}$$

where 2 ln 2 is the correction due to the gaussian-shaped beam.

By using the relationships in Eqs. (23.7) and (23.8), Eq. (23.12) can be written in terms of the reflectivity factor Z as

$$P_r = \frac{P_t G^2 \theta\phi c\tau \pi^3 |K|^2 Z}{512(2 \ln 2) r^2 \lambda^2} \tag{23.13}$$

One must be careful to use consistent units in Eq. (23.13). If meter-kilogram-seconds (mks) units are used, the calculation of Z from Eq. (23.13) will have dimensions of m^6/m^3. Conversion to the more commonly used units of mm^6/m^3 requires that the result be multiplied by the factor 10^{18}. Because Z values of interest can range over several orders of magnitude, a logarithmic scale is often used, where

$$\text{dBZ} = 10 \log Z \tag{23.14}$$

Equation (23.13) can be used to measure the reflectivity factor Z when the antenna beam is filled, when the Rayleigh approximation is valid, and when the scatterers are in either the ice or the water phase. Because all these conditions

are not always satisfied, it is common to use the term Z_e, the effective reflectivity factor, in place of Z. When Z_e is used, it is generally understood that the above conditions are assumed. Practitioners in the field of radar meteorology often use Z_e and Z interchangeably, albeit incorrectly.

Finally, it is important to note the range of Z values that are of meteorological significance. In nonprecipitating clouds, Z values as small as -40 dBZ are of interest. In the optically clear boundary layer, Z values of the order -20 dBZ to 10 dBZ are of interest. In rain, Z may range from about 20 dBZ to as much as 60 dBZ, with a 55 to 60 dBZ rain being of the type that can cause severe flooding. Severe hailstorms may produce Z values higher than 70 dBZ. Operational radars are generally designed to detect Z values ranging from 10 to 60 dBZ, while research applications usually aim for the maximum dynamic range possible. In light of the above, operational radars often employ sensitivity time control (STC) to compensate for inverse r^2 dependence, but research radars usually do not use STC owing to the attendant loss of sensitivity at short ranges.

23.3 DESIGN CONSIDERATIONS

Three of the more significant factors that affect the design of meteorological radars are attenuation, range-velocity ambiguities, and ground clutter. The combination of these three, along with the need to obtain adequate spatial resolution, leads to a wavelength selection in the range of 3 to 10 cm for most meteorological applications.

Attenuation Effects. Attenuation has at least two negative effects on meteorological radar signals. First, because of attenuation it becomes difficult, if not impossible, to make quantitative measurements of the backscattered energy from precipitation which is at greater range (and at the same azimuth and elevation angles) than precipitation closer to the radar. This inability to precisely measure the backscattering cross section makes quantitative measurements of precipitation rates more difficult.

Second, if the attenuation due to precipitation or the intervening medium is sufficiently great, the signal from a precipitation cell behind a region of strong absorption may be totally obliterated, leading to potentially disastrous effects. One example of the potentially serious consequences of very strong absorption is the impact it might have on airborne storm avoidance radars, most of which are in the 3-cm band, although some use a 5-cm wavelength. Metcalf[15] has examined ground-based radar data from the storm that was responsible for the 1977 crash of Southern Airways Flight 242 in northwest Georgia. The crew had relied on its on-board radar for penetration of a severe storm. Metcalf shows strong evidence that the region penetrated by the aircraft, while appearing to be free of echo, had actually been obliterated because of severe attenuation. Severe storms can also produce very strong absorption at 5-cm wavelength, as noted by Allen et al.[16]

In some meteorological radar applications, it is desirable to attempt to measure attenuation along selected propagation paths. This is done because absorption is related to liquid-water content and can provide useful information for the detection of such phenomena as hail, in accordance with the dual-wavelength technique described by Eccles and Atlas.[17]

In the following subsections, quantitative expressions relating attenuation to precipitation are given. Much of this is taken from Bean, Dutton, and Warner.[12]

Battan's textbook[10] is also an excellent source for additional information on the absorbing properties of precipitation.

Attenuation in Clouds. Cloud droplets are regarded here as those water or ice particles having radii smaller than 100 μm, or 0.01 cm. For wavelengths of incident radiation well in excess of 0.5 cm, the attenuation becomes independent of the drop-size distribution. The generally accepted equations for attenuation by clouds usually show the moisture component of the equations in the form of the liquid-water content (grams per cubic meter). Observations indicate that the liquid-water concentration in clouds generally ranges from[18] 1 to 2.5 g/m^3, although Weickmann and aufm Kampe[19] have reported isolated instances of cumulus congestus clouds with water contents of 4.0 g/m^3 in the upper levels. In ice clouds, it rarely exceeds 0.5 and is often less than 0.1 g/m^3. The attenuation due to cloud drops may be written[12]

$$K = K_1 M \tag{23.15}$$

where K = attenuation, dB/km
K_1 = attenuation coefficient, dB/(km · g · m^3)
M = liquid-water content, g/m^3

$$M = \frac{4\pi\rho}{3}\sum_{i=1}^{N} a_i^3 \tag{23.16}$$

$$K_1 = 0.4343\frac{6\pi}{\lambda}\mathrm{Im}\left(-\frac{m^2 - 1}{m^2 + 2}\right) \tag{23.17}$$

where the a_i are droplet radii, ρ is the density of water, and Im is the imaginary part. Values of K_1 for ice and water clouds are given for various wavelengths and temperatures by Gunn and East in Table 23.1.

Several important facts are demonstrated by Table 23.1. The decrease in attenuation with increasing wavelength is clearly shown. The values change by about an order of magnitude, for a change of λ from 1 to 3 cm. The data presented here also shows that attenuation in water clouds increases with decreasing temperature. Ice clouds give attenuations about two orders of magnitude smaller

TABLE 23.1 One-Way Attenuation Coefficient K_1 in Clouds in dB/(km · g · m^3)*

		Wavelength, cm			
Temperature, °C		0.9	1.24	1.8	3.2
Water cloud	20	0.647	0.311	0.128	0.0483
	10	0.681	0.406	0.179	0.0630
	0	0.99	0.532	0.267	0.0858
	−8	1.25	0.684	0.34 (extrapolated)	0.112 (extrapolated)
Ice cloud	0	8.74×10^{-3}	6.35×10^{-3}	4.36×10^{-3}	2.46×10^{-3}
	−10	2.93×10^{-3}	2.11×10^{-3}	1.46×10^{-3}	8.19×10^{-4}
	−20	2.0×10^{-3}	1.45×10^{-3}	1.0×10^{-3}	5.63×10^{-4}

*After Gunn and East.[20]

than water clouds of the same water content. The attenuation of microwaves by ice clouds can be neglected for all practical purposes.[10]

Attenuation by Rain. Ryde and Ryde[21] calculated the effects of rain on microwave propagation and showed that absorption and scattering effects of raindrops become more pronounced at the higher microwave frequencies, where the wavelength and the raindrop diameters are more nearly comparable. In the 10-cm band and at shorter wavelengths the effects are appreciable, but at wavelengths in excess of 10 cm the effects are greatly decreased. It is also known that suspended water droplets and rain have an absorption rate in excess of that of the combined oxygen and water-vapor absorption.[22]

In practice, it has been convenient to express rain attenuation as a function of the precipitation rate R, which depends on both the liquid-water content and the fall velocity of the drops, the latter in turn depending on the size of the drops.

Ryde[23] studied the attenuation of microwaves by rain and deduced, by using Laws and Parsons[24] distributions, that this attenuation in decibels per kilometer can be approximated by

$$K_R = \int_0^{r_0} [R(r)]^{\alpha} dr \tag{23.18}$$

where K_R = total attenuation, dB
K = function of frequency[25]
$R(r)$ = rainfall rate along path r
r_0 = length of propagation path, km
α = function of frequency[10]

Medhurst[26] shows that $\alpha = 1$ is a good assumption in many cases. The path loss per mile, according to Ryde, for the three carrier frequency bands of 4, 6, and 11 GHz, is shown in Fig. 23.1.

The greatest uncertainty in predictions of attenuation caused by rainfall, when theoretical formulas are used as a basis for calculation, is the extremely limited knowledge of drop-size distribution in rains of varying rates of fall under differing climatic and weather conditions. There is little evidence that a rain with a known rate of fall has a unique drop-size distribution, although studies on this problem seem to indicate that a certain most probable drop-size distribution can be attached to a rain of a given rate of fall.[27] Results of this study are shown in Table 23.2, which gives the percentage of total volume of rainfall occupied by raindrops of different diameters (centimeters) and varying rainfall rates (millimeters per hour). On the basis of these results, the absorption cross section of raindrops of different sizes is shown in Table 23.3. This table gives the decibel attenuation per kilometer in rains of different rates of fall for radio wavelengths between 0.3 and 10 cm.

Since the total-attenuation cross section[28] depends on the temperature (because of its effects on the dielectric properties of water), it is important to evaluate the attenuation of rains whose drops are at different temperatures from those in the preceding tables. Table 23.4 contains the necessary data relative to the change of attenuation with temperature and is to be used with Table 23.3.

To determine total attenuation caused by rainfall through a particular storm, something must be known about the nature of the storm itself and, consequently, about how its rainfall rates and drop sizes are distributed in three dimensions.

A systematic vertical variation of R, decaying with height above a measured surface value, seems to be appropriate in rainfall of a widespread (continuous) nature.[29] Widespread rainfall is usually triggered by a relatively large-scale mechanism, such as a frontal or monsoon situation. A vertical variation of R of the form

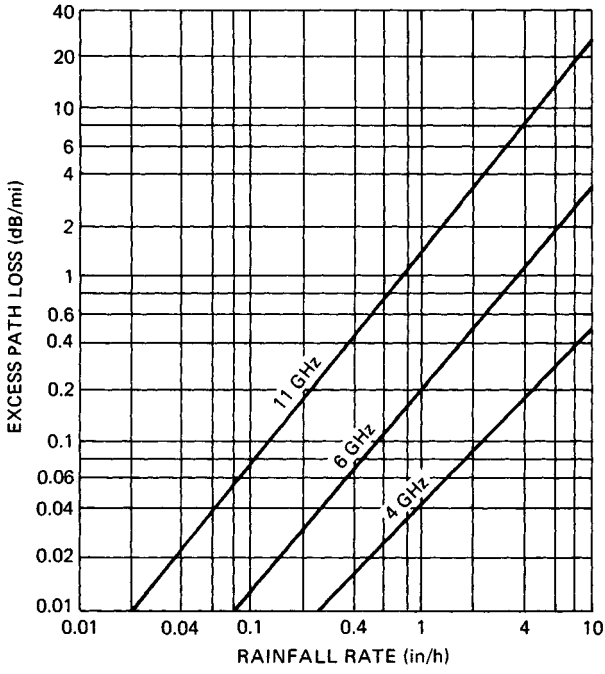

FIG. 23.1 Theoretical rain attenuation versus rainfall rate.

$$R = R_0 e^{-dh^2} \tag{23.19}$$

can be assumed to be appropriate under continuous-rainfall conditions.[29] In Eq. (23.19), R_0 is the surface rainfall rate, h is the height above the earth's surface, and d is a constant, equal to about 0.2.

Convective-type precipitation, however, shows a quite different nature. The presence of the *virga* (precipitation aloft but evaporating before reaching the surface) associated with so many shower-type clouds indicates that Eq. (23.19) is not especially representative of shower rainfall. Dennis[30] has done considerable work in examining rainfall determinations in shower-type activity. His observations show that the reflectivity factor $Z(\text{mm}^6/\text{m}^3)$ of an element of a vertical slice taken through a spherical shower cell is well represented by a regression line of the form

$$Z = c_1(r_0 - r)^{c_2} \tag{23.20}$$

In Eq. (23.20), r is the distance from the center of the cell of radius r_0, and c_1 and c_2 are positive constants.

Attenuation by Hail. Ryde[23] concluded that the attenuation caused by hail is one-hundredth of that caused by rain, that ice-crystal clouds cause no sensible attenuation, and that snow produces very small attenuation even at the excessive rate of fall of 5 in/h. However, the scattering by spheres surrounded by a concentric film of different dielectric constant does not give the same effect that

TABLE 23.2 Drop-Size Distribution*

Drop diameter D, cm	Precipitation rate p, mm/h							
	0.25	1.25	2.5	12.5	25	50	100	150
	Percentage of a given volume containing drops of diameter D							
0.05	28.0	10.9	7.3	2.6	1.7	1.2	1.0	1.0
0.10	50.1	37.1	27.8	11.5	7.6	5.4	4.6	4.1
0.15	18.2	31.3	32.8	24.5	18.4	12.5	8.8	7.6
0.20	3.0	13.5	19.0	25.4	23.9	19.9	13.9	11.7
0.25	0.7	4.9	7.9	17.3	19.9	20.9	17.1	13.9
0.30	.....	1.5	3.3	10.1	12.8	15.6	18.4	17.7
0.35	.....	0.6	1.1	4.3	8.2	10.9	15.0	16.1
0.40	.....	0.2	0.6	2.3	3.5	6.7	9.0	11.9
0.45	.....	.....	0.2	1.2	2.1	3.3	5.8	7.7
0.50	.....	.....	.....	0.6	1.1	1.8	3.0	3.6
0.55	.....	.....	.....	0.2	0.5	1.1	1.7	2.2
0.60	.....	.....	.....	.....	0.2	0.5	1.0	1.2
0.65	.....	.....	.....	.....	.....	0.2	0.7	1.0
0.70	.....	.....	.....	.....	.....	.....	.....	0.3

*From Burrows and Attwood.[27]

TABLE 23.3 Attenuation in Decibels per Kilometer for Different Rates of Rain Precipitation at Temperature 18°C*

Precipitation rate p, mm/h	Wavelength λ, cm								
	λ = 0.3	λ = 0.4	λ = 0.5	λ = 0.6	λ = 1.0	λ = 1.25	λ = 3.0	λ = 3.2	λ = 10
0.25	0.305	0.230	0.160	0.106	0.037	0.0215	0.00224	0.0019	0.0000997
1.25	1.15	0.929	0.720	0.549	0.228	0.136	0.0161	0.0117	0.000416
2.5	1.98	1.66	1.34	1.08	0.492	0.298	0.0388	0.0317	0.000785
12.5	6.72	6.04	5.36	4.72	2.73	1.77	0.285	0.238	0.00364
25.0	11.3	10.4	9.49	8.59	5.47	3.72	0.656	0.555	0.00728
50	19.2	17.9	16.6	15.3	10.7	7.67	1.46	1.26	0.0149
100	33.3	31.1	29.0	27.0	20.0	15.3	3.24	2.80	0.0311
150	46.0	43.7	40.5	37.9	28.8	22.8	4.97	4.39	0.0481

*From Burrows and Attwood.[27]

Ryde's results for dry particles would indicate.[23,31] For example, when one-tenth of the radius of an ice sphere of radius 0.2 cm melts, the scattering of 10-cm radiation is approximately 90 percent of the value that would be scattered by an all-water drop.

At wavelengths of 1 and 3 cm with $2a = 0.126$ (a = radius of drop), Kerker, Langleben, and Gunn[31] found that particles attained total-attenuation cross sections corresponding to all-melted particles when less than 10 percent of the ice particles was melted. When the melted mass reached about 10 to 20 percent, the attenuation was about twice that of a completely melted particle. These calculations show that the attenuation in the melting of ice immediately under the 0°C isotherm can be substantially larger than in the snow region just above and, under

TABLE 23.4 Correction Factor (Multiplicative) for Rainfall Attenuation*

Precipitation rate p, mm/h	λ, cm	0°C	10°C	18°C	30°C	40°C
0.25	0.5	0.85	0.95	1.0	1.02	0.99
	1.25	0.95	1.00	1.0	0.90	0.81
	3.2	1.21	1.10	1.0	0.79	0.55
	10.0	2.01	1.40	1.0	0.70	0.59
2.5	0.5	0.87	0.95	1.0	1.03	1.01
	1.25	0.85	0.99	1.0	0.92	0.80
	3.2	0.82	1.01	1.0	0.82	0.64
	10.0	2.02	1.40	1.0	0.70	0.59
12.5	0.5	0.90	0.96	1.0	1.02	1.00
	1.25	0.83	0.96	1.0	0.93	0.81
	3.2	0.64	0.88	1.0	0.90	0.70
	10.0	2.03	1.40	1.0	0.70	0.59
50.0	0.5	0.94	0.98	1.0	1.01	1.00
	1.25	0.84	0.95	1.0	0.95	0.83
	3.2	0.62	0.87	1.0	0.99	0.81
	10.0	2.01	1.40	1.0	0.70	0.58
150	0.5	0.96	0.98	1.0	1.01	1.00
	1.25	0.86	0.96	1.0	0.97	0.87
	3.2	0.66	0.88	1.0	1.03	0.89
	10.0	2.00	1.40	1.0	0.70	0.58

*From Burrows and Attwood.[27]

some circumstances, greater than in the rain below the melting level. Further melting cannot lead to much further enhancement, apparently, and may lead to a lessening of the reflectivity of the particle by bringing it to sphericity or by breaking up the particle. Melting of ice particles produces enhanced backscatter, and this effect gives rise to the radar-observed *bright band* near the 0°C isotherm.

Attenuation by Fog. The characteristic feature of a fog is the reduction in visibility. Visibility is defined as the greatest distance in a given direction at which it is just possible to see and identify with the unaided eye (1) in the daytime a prominent dark object against the sky at the horizon and (2) at night a known, preferably unfocused, moderately intense light source.[32]

Although the visibility depends upon both drop size and number of drops and not entirely upon the liquid-water content, in practice the visibility is an approximation of the liquid-water content and therefore may be used to estimate radio-wave attenuation.[33] On the basis of Ryde's work, Saxton and Hopkins[34] give the figures in Table 23.5 for the attenuation in a fog or clouds at 0°C temperature. The attenuation varies with the temperature because the dielectric constant of water varies with temperature; therefore, at 15 and 25°C the figures in Table 23.5 should be multiplied by 0.6 and 0.4, respectively. It is immediately noted that cloud or fog attenuation is an order of magnitude greater at 3.2 cm than at 10 cm. Nearly another order-of-magnitude increase occurs between 3.2 and 1.25 cm.

Range and Velocity Ambiguities. The unambiguous doppler frequency or Nyquist frequency for a fixed pulse-repetition-frequency (PRF) radar is given by

$$\Delta f = \pm \text{PRF}/2 \tag{23.21}$$

TABLE 23.5 Attenuation Caused by Clouds or Fog
Temperature = 0°C*

	Attenuation, dB/km		
Visibility, m	λ = 1.25 cm	λ = 3.2 cm	λ = 10 cm
30	1.25	0.20	0.02
90	0.25	0.04	0.004
300	0.045	0.007	0.001

*From Saxton and Hopkins.[34]

where PRF is the pulse repetition frequency. The unambiguous range interval is given by

$$\Delta r = \frac{c}{2\text{PRF}} \tag{23.22}$$

and the product $\Delta f \Delta r$ is simply

$$\Delta f \Delta r = \frac{c}{2} \tag{23.23}$$

Since the doppler shift f and the target radial velocity v are linearly related by the expression

$$v = \frac{\lambda}{2} f \tag{23.24}$$

it follows that the product of unambiguous velocity and unambiguous range is

$$\Delta v \Delta r = \frac{\lambda c}{4} \tag{23.25}$$

and is maximized by maximizing λ, the transmitted wavelength.

Ground Clutter Effects. Many meteorological radar applications call for the detection of precipitation echoes in the presence of ground clutter. Airborne weather radars during takeoff or landing are particularly susceptible. Another application, in which ground clutter is serious, relates to the detection of low-level wind shear.

While ground clutter cannot be eliminated, its effects can be mitigated through careful design. The most straightforward approach is to use antennas with low sidelobes, particularly in elevation. A second approach is through the use of shorter wavelengths. Shorter wavelengths result in improved signal-to-clutter ratios owing to the fact that the backscattered weather signal power is inversely proportional to λ^4 while the ground clutter return is only weakly dependent on wavelength. If one assumes that the clutter signal is wavelength-independent and the antenna beamwidth is fixed, Eq. (23.13) may be used to show that the weather-signal-power to clutter-power ratio is inversely proportional to λ^2.

Typical Weather Radar Designs. There is no universal weather radar system design that can serve all purposes. Airborne weather radars are constrained by size and weight limitations. Ground-based radars may be constrained by cost considerations. Severe storm warning radars require long range and high unambiguous velocity, and they must penetrate very heavy rain, thus dictating long wavelengths. Radars designed for studies of nonprecipitating clouds may use short wavelengths[35,36] (8 mm or even 3 mm) in order to achieve sufficient sensitivity to detect small cloud particles of the order of 100 μm and smaller. And FM-CW radars[37] have been used to obtain very-high-range resolution for detection of very thin layers in the clear air.

However, most meteorological radars are conventional pulsed or pulsed doppler systems. Ground-based radars used for severe storm research or warning will normally use S-band (≈3 GHz) or C-band (≈5.5 GHz) transmitters. Airborne storm avoidance radars will use either C-band or X-band (≈10 GHz) transmitters.

A 1° beamwidth is commonly used for longer-range radars. Admittedly, this is somewhat arbitrary, but the choice of 1° is based upon several decades of experience. A 1° beam will provide resolution of 2 km at a range of 120 km. Because thunderstorms contain important spatial features, such as heavy precipitation shafts and updraft cores, with horizontal dimensions of the order 1 to 5 km, a 1° beam is reasonably well matched to the phenomena being observed. Shorter-range and airborne weather radars often employ beamwidths of between 2 and 3°.

Operational weather radars normally are capable of short- and long-pulse operation in the range of 0.5 μs to about 6 μs. Through pulse-width diversity, high resolution is obtained, usually at short range, while for long-range detection longer pulses provide increased sensitivity and tend to equalize the along-beam and cross-beam resolutions.

Equation (23.13) shows that the received power is directly proportional to the pulse width τ. The noise power N is conventionally given by

$$N = \kappa TB \tag{23.26}$$

where κ = Boltzmann's constant, 1.38×10^{-23} W/(H$_z$ · K)
T = receiver noise temperature, K
B = receiver noise bandwidth

For a matched receiver

$$B \approx \frac{1}{\tau} \tag{23.27}$$

The signal-to-noise ratio is therefore given by the proportionality

$$\frac{P_r}{N} \propto \frac{\tau}{\kappa TB} \approx \frac{\tau^2}{\kappa T} \tag{23.28}$$

Thus, for distributed targets and with the pulse volume filled with scatterers, the signal-to-noise ratio for a single pulse is proportional to the pulse width squared. This assumes that the peak power is unchanged and that the average power increases linearly with τ. If the transmitter's average power is fixed, the signal-to-noise ratio will be proportional to τ.

PRFs for meteorological radars range from as low as several hundred s^{-1} for

long-range detection to several thousand s^{-1} for shorter-wavelength systems attempting to achieve high unambiguous velocities. Generally speaking, most meteorological doppler radars are operated in a single mode, compromising the radar's ability to unambiguously resolve either range or velocity. More recent designs, however, may use a dual pulse repetition period[38] (PRT) to resolve both range and velocity. Another approach[39] is to employ a transmitted-pulse sequence with random phases from pulse to pulse. Range ambiguities cannot be totally eliminated, but their effects can be significantly mitigated through these approaches.

To discuss design details of all types of meteorological radars is beyond the scope of this chapter. However, it will be useful to include some of the important characteristics of the NEXRAD radar, which illustrate the performance of a modern operational weather radar ca. 1989. Table 23.6 contains some of the more relevant NEXRAD design features.

TABLE 23.6 Some Relevant NEXRAD System Characteristics

Transmitted power (klystron)	700,000 W
Pulse width	1.6, 4.8 μs
Range (doppler mode)	230 km
Unambiguous velocity (doppler mode)	±50 m/s
Range (nondoppler mode)	460 km
Clutter rejection	50 dB
Beamwidth	1°
System sensitivity	(−8 dBZ at 50 km)

23.4 SIGNAL PROCESSING

It can be shown[8,11] that the received signal from meteorological targets is well represented by a narrowband gaussian process. This is a direct consequence of the fact that (1) the number of scatterers in the pulse volume is large ($>10^6$); (2) the pulse volume is large compared with the transmitted wavelength; (3) the pulse volume is filled with scatterers, causing all phases on the range from 0 to 2π to be returned; and (4) the particles are in motion with respect to one another due to turbulence, wind shear, and their varying fall speeds.

The superposition of the scattered electric fields from such a large number of particles (each with random phase) gives rise, through the central limit theorem, to a signal with gaussian statistics. Because the particles are in motion with respect to one another, there is also a doppler spread, often referred to as the variance of the doppler spectrum. Finally, since all the particles within the sample volume are moving with some mean or average radial velocity, there is a mean frequency of the doppler spectrum which is shifted from the transmitted frequency.

The power spectral density of a meteorological signal is depicted schematically in Fig. 23.2 and can be interpreted as follows. The received power is simply the integral under the curve and is given by

$$P_r = \int S(f)df = \int S(v)dv \tag{23.29}$$

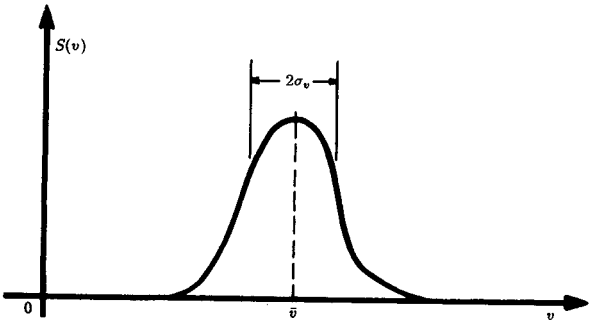

FIG. 23.2 The doppler spectrum. Received power, radial velocity, and spectrum width can be calculated and are directly related to meteorological variables.

where f and v are related by $f = (2/\lambda)v$.

The mean velocity is given by the first moment of the spectrum

$$\bar{v} \frac{\int vS(v)dv}{\int S(v)dv} \tag{23.30}$$

The second central moment σ_v^2 is given by

$$\sigma_v^2 \frac{\int (v - \bar{v})^2 S(v)dv}{\int S(v)dv} \tag{23.31}$$

where σ_v is the velocity width. Radar meteorologists refer to σ_v^2 as the spectrum variance because of its computational equivalence to the variance of a continuously distributed random variable. In short, $S(v)$ is analogous to a probability density function for v. The term *spectrum variance* will be used to refer to σ_v^2, and the term *spectrum width* to refer to σ_v. It is clear, therefore, that the doppler spectrum contains the information necessary to measure important signal parameters.

In the most general case, quadrature phase detection is used to obtain the real and imaginary parts of the complex signal envelope.[8] These are usually digitized in a large number of range gates ($\approx$1000) at the radar's pulse repetition frequency. The resultant complex time series in each gate can then be processed by using a fast Fourier transform (FFT) to obtain an estimate of the doppler spectrum from which the mean velocity and spectrum variance can be obtained.

A more efficient estimation technique is described by Rummler.[40] This estimator makes use of the fact that the complex autocorrelation function of the signal has the general form

$$R(x) = P_r \rho(x) e^{j\frac{4\pi\bar{v}}{\lambda}x} \tag{23.32}$$

where $\rho(x)$ is the correlation coefficient and x is a dummy variable.

It follows that $\bar{v}$, the mean velocity, is given by

$$\bar{v} = \frac{\lambda}{4\pi x} \arg [R(x)] \tag{23.33}$$

It can also be shown that

$$\sigma_v^2 \approx \frac{\lambda^2}{8\pi^2 x^2}\left[1 - \frac{R(x)}{R(o) - N}\right] \tag{23.34}$$

where N is the noise power.

This estimator is widely used for mean-frequency estimation with doppler meteorological radars. The estimates are unbiased in the presence of noise when the doppler spectrum is symmetrical. Its greatest appeal, however, is due to its computational simplicity. For a pulsed radar, with a pulse repetition period (PRT) T, $R(T)$ is obtained from the simple expression[8]

$$R(T) = \frac{1}{N}\sum_{(k=0)}^{(N-1)} s_{k+1} s_k^* \tag{23.35}$$

where the s_k are the complex signal samples (sampled at the radar PRT) in a given range gate and s_k^* is the complex conjugate. It is clear that this algorithm requires only N complex multiplications for a time series of N samples while the FFT requires $N \log_2 N$. This *pulse-pair algorithm*, as it is often called, therefore not only is an excellent estimation technique but is less complex and costly than comparable FFT processors. In addition, FFT estimates of mean velocity and spectrum width are biased by receiver noise. If the FFT approach is used, the bias due to noise can be removed by estimating the noise threshold in the spectral domain and truncating the derived spectrum.[41]

For most applications, the pulse-pair processor has become the technique of choice. However, in some research applications it remains advantageous to have access to the full doppler spectrum. Very fast and programmable digital signal-processing chips make it possible for radar meteorologists to have their cake and eat it too. Flexibility due to programmability permits tailoring of the processor's characteristics to the application from day to day or even beam to beam and range gate to range gate. Until recently, most pulse-pair or FFT processors for meteorological radars have been hard-wired and therefore inflexible.

Measurement Accuracy. Because the received signals are sample functions from gaussian random processes, the doppler spectrum and its moments cannot be measured exactly in any finite period of time. Consequently, all measurements will be somewhat in error, with the error being a function of the properties of the atmosphere, the radar wavelength, and the time allocated to the measurement.

The theoretical development of signal estimator statistics is found in Denenberg, Serafin, and Peach[42] for the FFT technique. Doviak and Zrnić[11] cover the subject quite completely. Following are some useful expressions for the mean square error of mean power and mean velocity estimates.

Power Estimation. It is well known that for a gaussian process,[43] using square-law signal detection, samples of the mean power P_r of the process are exponentially distributed with variance P_r^2. Given a time T_0 allocated to the measurement and a signal bandwidth σ_f(Hz), there will be approximately $\sigma_f T_0$ independent samples of the square of the signal envelope. It follows, therefore, that an estimate $\hat{P}_r$ of the mean power for this process will have a variance or mean square error given by

$$\text{var}\,(\hat{P}_r) \approx \frac{P_r^2}{\sigma_f T_0} \tag{23.36}$$

Substituting for σ_f from the expression $\sigma_f = 2\sigma_v/\lambda$, where σ_v is the width of the doppler spectrum, Eq. (23.36) becomes

$$\text{var}\,(\hat{P}_r) \approx \frac{\lambda P_r^2}{2\sigma_v T_0} \tag{23.37}$$

This expression is valid for high signal-to-noise cases.

Velocity Estimation. Denenberg, Serafin, and Peach[42] give the following expression for the variance of mean-frequency estimates of the doppler spectrum

$$\text{var}(\hat{f}) = \frac{1}{P_r^2 T_0}\int f^2 S^2(f + \bar{f}\,)df \tag{23.38}$$

This is an interesting result, showing that the variance of the estimate $\hat{f}$ is a function only of the shape of the doppler spectrum and the integration time T_0. If the spectrum has a gaussian shape, with variance σ_f^2, Eq. (23.38) becomes

$$\text{var}(\hat{f}) = \frac{\sigma_f}{4\sqrt{\pi} T_0} \tag{23.39}$$

Noting that $\text{var}(\hat{v}) = (\lambda/2)^2\ \text{var}\,(\hat{f})$, we can write

$$\text{var}\,(\hat{v}) = \frac{\lambda\sigma_v}{8\sqrt{\pi} T_0} \tag{23.40}$$

If we multiply numerator and denominator by σ_v, Eq. (23.40) becomes

$$\text{var}(\hat{v}) = \frac{\lambda\sigma_v^2}{8\sqrt{\pi}\sigma_v T_0} = \frac{\sigma_v^2}{4\sqrt{\pi}\sigma_f T_0} \tag{23.41}$$

Thus, it is seen that the variance of the mean velocity estimate $\hat{v}$ is directly proportional to the variance of the doppler spectrum and inversely proportional to the number of independent samples. Note also that var $(\hat{v})$ is proportional to λ, indicating that, for the same processing time T_0 and for the same σ_v, the variance of the estimate can be reduced by reducing the wavelength, which increases the number of independent samples.

Equations (23.38), (23.39), (23.40), and (23.41) are applicable in high signal-

to-noise-ratio cases. Zrnić[44] gives the following expression for the variance of the mean-frequency estimate $\hat{f}$ for the pulse-pair estimation technique and a gaussian-shaped spectrum

$$\text{var}(\hat{f}) = \frac{1}{8\pi^2 T_0 \rho^2(T) T}\left\{2\pi^{3/2}\sigma_f T + \frac{N^2}{S^2} + 2\frac{N}{S}[1 - \rho(2T)]\right\} \tag{23.42}$$

where ρ is the correlation coefficient and N/S is the noise-to-signal ratio. Equation (23.42) applies to a single PRF with interpulse period T and assumes that all pulses in the interval T_0 are used in the estimation algorithm. It reduces exactly to Eq. (23.39) for large S/N and for narrow spectra, i.e., $\rho(T) \approx 1$. The reader is referred to Zrnić[44] for further details regarding the estimation of other moments of the doppler spectrum.

Processor Implementations. In nondoppler radars it is common to use log-video receivers along with sensitivity time control (STC) for inverse r^2 correction in order to achieve the widest dynamic range possible. For signal power estimation, the log-video signal is digitized and averaged or, in the most rudimentary of systems, may be used to modulate an analog PPI or other type of radarscope directly. Most modern meteorological radars, however, use digital averaging along with digital color displays for added quantitative precision. Note that when the logarithm is averaged, the estimate will be biased downward by as much as 2.5 dB.[45] This bias must be removed in order to accurately estimate the received signal power.

For doppler radars it has been common to use both linear and logarithmic receivers, with the log channel used for reflectivity estimation and the linear channel for doppler parameter estimation. This approach, however, often results in saturation of the linear channel and therefore some distortion of the doppler spectrum.[46]

Most modern designs now attempt to maintain linearity in the receiver through the use of a dynamic automatic gain control (AGC), whereby the receiver gain is adjusted from range gate to range gate through the use of rapidly switched attenuators. The estimate needed to select the proper attenuator may come from an independent log channel or may be based upon a short segment of the signal. Another approach[47] is to delay the signal for a period of the order of a microsecond while an estimate of signal strength can be made and the proper attenuator setting can be established. Clearly, such rapid switching in the receiver requires careful design in order to avoid the effects of switching transients. An approach that avoids transient effects is to use parallel IF strips, each with moderate dynamic range and fixed gains, and to sample the signal in the channel that is best matched to the signal strength.

In all these approaches, it is possible to achieve wide linear dynamic range of the order of 80 dB or greater and to use floating-point digital arithmetic. The reflectivity, mean doppler velocity, and spectrum width can all be estimated digitally from the floating-point linear channel samples.

23.5 OPERATIONAL APPLICATIONS

As has been demonstrated, meteorological radars measure backscattered power and radial velocity parameters. The challenge to the radar meteorolo-

gist is to translate these measurements, their spatial distributions, and their temporal evolution into quantitative assessments of the weather. The level of sophistication used in interpretation varies broadly, ranging from human interpretation of rudimentary gray-scale displays to computer-based algorithms and modern color-enhanced displays to assist human interpreters. Expert system approaches[48] that attempt to reproduce human interpretive logical processes can be employed effectively. Baynton et al.,[49] Wilson and Roesli,[50] and Serafin[1] all show how modern meteorological radars are used for forecasting the weather. The degree to which automation can be applied is evident in the NEXRAD radar system design, where the meteorological products shown in Table 23.7 will be automated.[51]

TABLE 23.7 NEXRAD Automated Products

Doppler radar data archive of storm phenomena
Precipitation analysis
Wind analysis
Tornado analysis
Fine-line analysis
Tropical cyclone analysis
Mesocyclone analysis
Thunderstorm analysis
Turbulence analysis
Icing analysis
Hail analysis
Freezing-melting analysis
Interpretive techniques
Multiple-radar mosaics

Precipitation Measurement. Among the more important parameters to be measured is rainfall, having significance to a number of water resource management problems related to agriculture, fresh-water supplies, storm drainage, and warnings of potential flooding.

The rainfall rate can be empirically related to the reflectivity factor[12] by an expression of the form

$$Z = aR^b \tag{23.43}$$

where a and b are constants and R is the rainfall rate, usually in millimeters per hour. Battan[10] devotes three full pages of his book to the listing of dozens of Z-R relationships derived by investigators at various locations throughout the world, for various weather conditions and in all seasons of the year. The fact that no universal expression can be applied to all weather situations is not surprising when one notes that rainfall drop-size distributions are highly variable. For many conditions,[10] the drop-size distribution can be represented by an exponential function

$$N(D) = N_0 e^{-\Lambda D} \tag{23.44}$$

where N_0 and Λ are constants. If $N(D)$ is known, the reflectivity factor can be calculated from Eq. (23.9). By using the terminal-fall speed data of Gunn and Kinzer,[52] the rainfall rate can also be obtained and Z directly related to R.

Clearly, a single-wavelength, single-polarization radar can measure only a single parameter Z and must assume Rayleigh scattering. Since the rainfall rate depends upon two parameters, N_0 and Λ, it is not surprising that Eq. (23.43) is nonuniversal. Despite this fact, Battan[10] lists four expressions as being "fairly typical" for the following four types of rain:

$$\text{Stratiform rain}^{53} \quad Z = 200\,R^{1.6} \tag{23.45}$$

$$\text{Orographic rain}^{54} \quad Z = 31\,R^{1.71} \tag{23.46}$$

$$\text{Thunderstorm rain}^{55} \quad Z = 486\,R^{1.37} \tag{23.47}$$

$$\text{Snow}^{56} \quad Z = 2000\,R^{2} \tag{23.48}$$

Stratiform refers to widespread, relatively uniform rain. *Orographic* rain is precipitation that is induced or influenced by hills or mountains. In each of the above expressions, Z is in mm^6/m^3 and R is in mm/h. In Eq. (23.48), R is the precipitation rate of the melted snow.

For a more complete treatment of this topic, the reader is referred to Battan.[10] Wilson and Brandes[57] give a comprehensive treatment of how radar and rain-gauge data can be used to complement one another in measurements of precipitation over large areas. Bridges and Feldman[58] discuss how two independent measurements (reflectivity factor and attenuation) can be used to obtain both parameters of the drop-size distribution and therefore precisely determine the rainfall rate. Seliga and Bringi[59] show how the measurement of Z at horizontal and vertical polarization also can produce two independent measurements and therefore provide more accurate rainfall rate measurements. Zawadzki[60] argues, however, that other factors contribute far more to the variability of precipitation rate than does the drop-size distribution. He states, therefore, that dual-parameter estimation techniques are not likely to be successful in many cases. Wilson and Brandes[57] state that cumulative precipitation measurements with radar, in storm situations, can be expected to be accurate to a factor of 2 for 75 percent of the time. Accuracies over large areas can be improved to about 30 percent with the addition of a surface rain-gauge network. It is this author's opinion that no single topic in radar meteorology has received more attention than rainfall rate measurement. Although useful empirical expressions have evolved, a completely satisfactory approach remains to be discovered.

Severe Storm Warning. One of the primary purposes of weather radars is to provide timely warnings of severe weather phenomena such as tornadoes, damaging winds, and flash floods. Long-term forecasting of the precise location and level of severity of these phenomena, through numerical weather prediction techniques, is beyond the state of the art. Operational radars, however, can detect these phenomena and provide warnings (of up to 30 min) of approaching severe events; they can also detect the rotating mesocyclones in severe storms that are precursors to the development of tornadoes at the earth's surface.[61]

Tornado Detection. A single doppler radar can only measure the radial component of the vector wind field. Hence, exact measurements of vector winds at a point are generally not possible. However, rotating winds or vortices can be detected and their intensities measured by simply measuring the change in radial

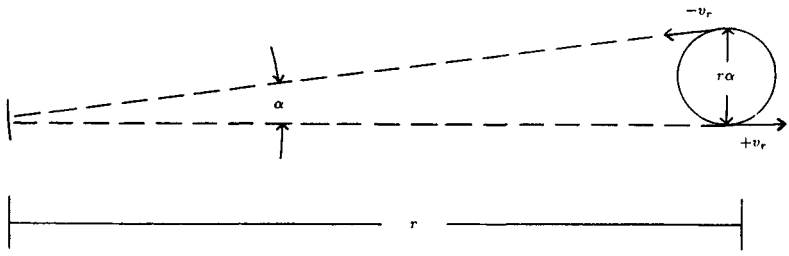

FIG. 23.3 Measurement of rotation or azimuthal shear in a mesocyclone. The azimuthal shear is given by $\Delta v/\Delta x = 2v_r/r\alpha$.

velocity with azimuth angle as shown in Fig. 23.3. The radar scans in azimuth and detects a couplet in radial velocity at constant range. The azimuthal shear is given simply by the expression

$$\frac{dv_r}{dx} \approx \frac{2v_r}{r\alpha} \tag{23.49}$$

where x is in the direction orthogonal to the radius r and d is the angle subtended by the circulation at range r.

Because mesocyclones, which spawn tornadoes, can be many kilometers in diameter, radars with 1° beams have the spatial resolution to detect mesocyclones at ranges in excess of 60 km. It should be clear that any mean translational motion would change the absolute values of the measured radial velocities but would not affect the shear measurement. Armstrong and Donaldson[62] were the first to use shear for severe storm detection. Azimuthal shear values of the order of 10^{-2} s^{-1} or greater and with vertical extent greater than the diameter of the mesocyclone are deemed necessary for a tornado to occur.[63]

Detection of the tornado vortex itself is not generally possible, since its horizontal extent may be only a few hundred meters. Detection of the radial shear, therefore, is not possible unless the tornado is close enough to the radar to be resolved by the beamwidth. In cases where the tornado falls entirely within the beam, the doppler spectral width[64] may be used to estimate tornadic intensity. In some cases, both a mesocyclone and its incipient tornado can be detected. Wilson and Roesli[50] show an excellent example of a tornado vortex signature (TVS) embedded within a larger mesocyclone.

Microbursts. Fujita and Caracena[65] first identified the microburst phenomenon as the cause of an airliner crash that took place in 1975. The microburst and its effects on an aircraft during takeoff or landing are depicted in Fig. 23.4. The microburst is simply a small-scale, short-duration downdraft emanating from a convective storm. This "burst" of air spreads out radially as it strikes the ground, forming a ring of diverging air about 0.3 to 1 km deep and of the order of 2 to 5 km in diameter. Aircraft, penetrating a microburst, experience first an increase in head wind and then a continuous, performance-robbing decrease in head wind, which can cause the plane to crash if encountered shortly before touchdown or just as the aircraft is taking off. More complete descriptions of microbursts and their effects on aviation safety are given by Fujita[66,67] and McCarthy and Serafin.[68]

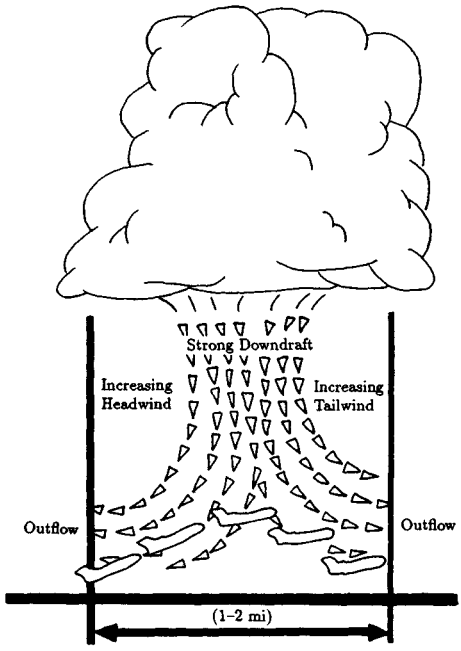

FIG. 23.4 Artist's depiction of a microburst and its effect on an aircraft during takeoff. The loss of airspeed near to the ground can be extremely hazardous.

Microburst detection, like tornado detection, is accomplished by estimating shear. However, in the case of the microburst, it is the radial shear of the radial velocity that is typically measured. Human interpretation of microburst signatures in color-enhanced radial velocity displays is easily accomplished with trained observers.[50] Radial velocity differences of 10 to 50 m/s are observed in microbursts. A radial velocity difference of 25 m/s over the length of a jet runway (≈3 km) is of serious concern.

One principal problem concerning microbursts is their short lifetimes, which are of order 15 min. The duration of peak intensity is only 1 or 2 min. The Classify, Locate, and Avoid Wind Shear (CLAWS) project[69] in 1984 clearly demonstrated that a 2-min advance warning using doppler radar and human interpreters can be achieved. The use of doppler radars operationally, however, will require completely automated detection algorithms. A second major problem is ground clutter. Since the phenomenon occurs near the ground and oftentimes in very light or no precipitation, ground clutter mitigation is necessary.

C band seems to be the preferred operational frequency for several reasons. First, a C-band antenna will be physically smaller than an S-band antenna for the same beamwidth, an important consideration for use near airports. Second, since long-range detection is not of importance, attenuation effects are not of primary concern. Third, C band offers improved signal-to-clutter performance. X band is not the frequency of choice owing to more serious range-velocity ambiguities and the more severe attenuation that can occur in very heavy rain. It is expected that deployment of a national network of doppler radars near airports will begin in the early 1990s.

Hail. The NEXRAD radar will make use of a hail-detection algorithm similar to that discussed by Witt and Nelson.[70] This algorithm combines high reflectivity factor with echo height and upper-level radial velocity divergence to detect the occurrence of hail. Eventually, polarization diversity techniques may improve quantitative hail detection. Aydin, Seliga, and Balaji[71] propose a hail-detection technique using reflectivity measurements at orthogonal polarizations. This technique depends upon the fact that the ratio of horizontal to vertical reflectivity is unity ($\approx$0 dB) when hail is present. This differs sharply from heavy rain, where this ratio can be as large as 6 dB. The combination of absolute reflectivity factor at horizontal polarization and ratio of reflectivities at horizontal and vertical polarizations (differential reflectivity) gives unique signatures for hail and heavy rain, each of which is characterized by high reflectivity factor. The difference in the differential reflectivity signatures is easily explained. Large raindrops assume pancakelike shapes as they fall and thus scatter back horizontally polarized electric fields more strongly than vertically polarized electric fields. Hailstones, while irregular in shape, appear to tumble while they fall and therefore exhibit no preferred orientation on average.

Wind Measurement. Lhermitte and Atlas[72] were the first to show how a single doppler radar can be used to measure vertical profiles of horizontal wind. This technique can be used if the precipitation and the wind are uniform in the region scanned by the radar. The method depends upon an analysis of the radial velocity measured during a complete scan in azimuth with elevation angle fixed. At any slant range r, the diameter of the region scanned is $r \cos \alpha$, and the height of the measurement is $r \sin \alpha$, where α is the elevation angle (see Fig. 23.5). If β is the azimuth angle, V_h is the horizontal wind speed, and V_f is the fall speed of the particles, the radial velocity at range r is given by

$$V_r(\beta) = V_h \cos \beta \cos \alpha + V_f \sin \alpha \tag{23.50}$$

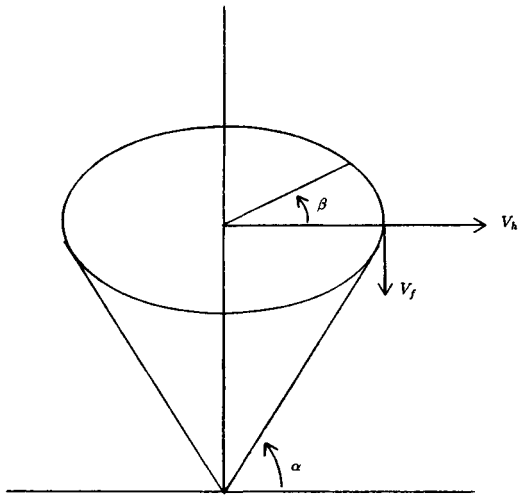

FIG. 23.5 Velocity-azimuth-display geometry for measuring horizontal wind with a single doppler radar. Measurement of the radial velocity for a complete azimuthal scan (β) permits measurement of horizontal winds.

A harmonic analysis can be used to obtain V_h, the horizontal wind speed, the wind direction, and V_f, the particle fall speed. The technique is referred to as the velocity-azimuth-display (VAD) technique. Browning and Wexler[73] later showed how the technique could be extended to measure other parameters of the wind field including divergence and deformation. Baynton et al.[49] show how the VAD can be applied in real time by using a color-enhanced radial velocity display.

Thunderstorm Prediction. Wilson and Schreiber[74] illustrate how modern meteorological doppler radar can be used to detect locations where new thunderstorm development is likely to occur. Modern radars have sufficient sensitivity to detect clear-air discontinuities in the lower 2 to 4 km of the atmosphere. Principally, this detection occurs in the summer months. The backscattering mechanism may be due to index-of-refraction inhomogeneities caused by turbulence in the lower layers and/or by insects. Wilson and Schreiber have found that about 90 percent of the thunderstorms that occur in the Front Range of the Rockies in the summertime develop over such boundaries. Since these boundaries can be detected before any clouds are present and because it is possible to infer the air mass convergence that is taking place along these boundaries through doppler measurements, more precise prediction of thunderstorm occurrence appears to be possible. From the radar designer's standpoint, such applications dictate the use of antennas with very low sidelobes and signal processors with significant ground clutter rejection capability. The NEXRAD radar system, with 50 or more dB of clutter rejection, is well suited to this eventual operational task.

23.6 RESEARCH APPLICATIONS

Operational meteorological radars are designed for reliability and simplicity of operation while providing the performance needed for operational applications. Research radars are considerably more complex, since cutting-edge research requires more detailed and more sensitive measurements of a multiplicity of variables simultaneously. In the research community, multiple-parameter radar studies, multiple-doppler radar network studies, and plans for airborne and spaceborne radars are all receiving considerable attention.

Multiple-Parameter Radar. It has been noted earlier that doppler radar provides a significant increase in the useful information that can be obtained from meteorological targets. The detection of hail, through the use of polarization diversity, adds additional information, and multiple wavelength provides yet another input related to the eventual interpretation of the size, water-phase state, and types of hydrometeors in all classes of clouds and precipitation. Very-short-wavelength radars are useful for probing newly developing clouds, while longer-wavelength radars are necessary for the study of severe storms. Researchers often need a wide range of these capabilities simultaneously. The capabilities desired of multiple-parameter meteorological radars are presented in the collection of papers edited by Hall.[6]

From the radar engineering standpoint, the challenge is considerable, requiring radar designers to develop fully coherent, polarization-diverse, and wavelength-diverse radars. Figure 23.6 is a photograph of the S (10-cm)- and X (3-cm)-band polarization-diverse doppler radar operated by the National Center for Atmospheric Research (NCAR). The system permits simultaneous measurements of the reflectivity factor on 2 wavelengths—the doppler parame-

FIG. 23.6 The CP-2, multiple-parameter radar at the National Center for Atmospheric Research, Boulder, Colorado. (*Courtesy of the National Center for Atmospheric Research.*)

ters on a single wavelength, S band, and polarization-diverse measurements at both wavelengths. The antenna beams are matched with approximately 1° beamwidths. The peak transmitted power at S band is 1 MW and 50 kW at X band. The pulse widths are approximately 1 μs, and the PRF is typically 1000 s^{-1}. The system is characteristic of the technologies currently in place in the research community in this field.

Multiple Radars. A single doppler radar measures only a single radial component of velocity. Lhermitte[3] was among the first to describe how two or more doppler radars could be used, scanning together, to obtain the full three-dimensional air motion fields in precipitation. This pioneering work led the way toward the use of networks of doppler radars for studies of individual clouds and larger-scale cloud systems. For the first time, it became possible to examine the three-dimensional structure of vector air motion in precipitation. Figure 23.7 illustrates an air motion field obtained by multiple-doppler radar observations in an individual convective storm cell. Shown are the horizontal

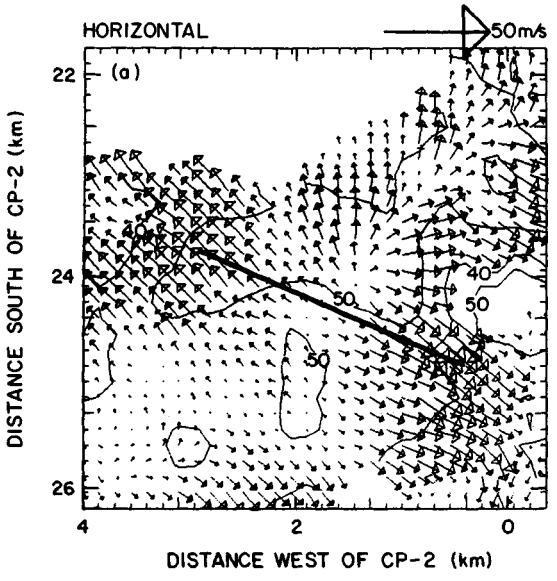

FIG. 23.7 Vector wind fields in a horizontal plane derived from dual-doppler radar observations of a summertime convective storm near Denver, Colorado. The divergent outflow is from a microburst. The dark, solid line is shown to indicate the length of a typical jet aircraft runway. (*Courtesy of the National Center for Atmospheric Research.*)

vector fields in a plane approximately 100 m above the surface. The phenomenon being measured is a low-level divergent outflow (or microburst). Figure 23.8 shows another example of air motion fields in a vertical plane orthogonal to an intense squall line in California.[75]

Rapid Scanning. The use of multiple-doppler radars has provided dramatic new information on the internal winds in large precipitating systems—information that can be obtained in no other way. Despite the power of this technique, the spatial resolution in the derived three-dimensional motion fields is generally not better than of the order of 2 km. The reasons for this are several. The finite beamwidth limits the resolution available at longer ranges. At shorter ranges, the large solid angle that must be scanned in order to cover all regions of a storm requires total scanning times of the order of 3 to 5 min even for ideally situated storms. This is a consequence of the on-target time necessary for accurate radial velocity measurements. Finally, the storm itself is evolving and moving during this measurement time.

Some research applications require faster scanning. These applications include the study of finer-scale storm features, interactions between the kinematics and hydrometeor growth processes in the storms, and studies of electric-charge separation in clouds. Brook and Krehbiel[76] were the first to discuss a very-rapid-scanning radar (although nondoppler) for effectively obtaining snapshots of convective storms. Keeler and Frush[77] discuss design considerations for a rapid-scanning doppler radar. Any rapid-scanning approach generally must encompass

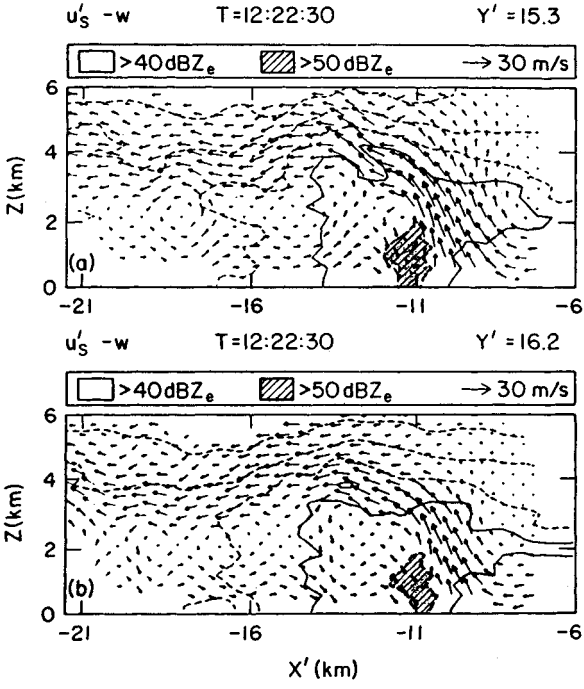

FIG. 23.8 Vertical cross sections of vector air motion in planes orthogonal to a California wintertime squall line.[75]

two features: (1) there must be relatively broadband transmissions to increase the independent samples available within the spatial resolution cell, thus reducing the dwell time; and (2) the antenna must be scanned—either very rapidly mechanically or electronically. An alternative approach might use several simultaneous beams and receivers.

Airborne and Space-Borne Radars. Hildebrand and Mueller[4] and Mueller and Hildebrand[5] have quantitatively demonstrated that it is possible for an airborne meteorological doppler radar to measure internal kinematic fields that are comparable to those obtained from ground-based systems. This powerful technique permits the use of a mobile platform, which therefore allows measurements over regions not accessible by ground-based systems. Moreover, the mobility of the aircraft permits longer-term observations of rapidly moving but long-lived storms and cloud systems. Figure 23.9 shows a photograph of the antenna of the airborne doppler radar mounted on the tail of the P-3 aircraft operated by the National Oceanic and Atmospheric Administration (NOAA). The antenna, covered by a cylindrical radome in flight, scans in range-height-indicator (RHI) mode, in vertical planes orthogonal to the aircraft fuselage. The aircraft is flown on orthogonal tracks in order to synthesize dual-doppler observations and therefore to obtain vector winds.

A point should be made here regarding the use of two doppler radars for measurements of three-dimensional winds. Since in principle two independent looks

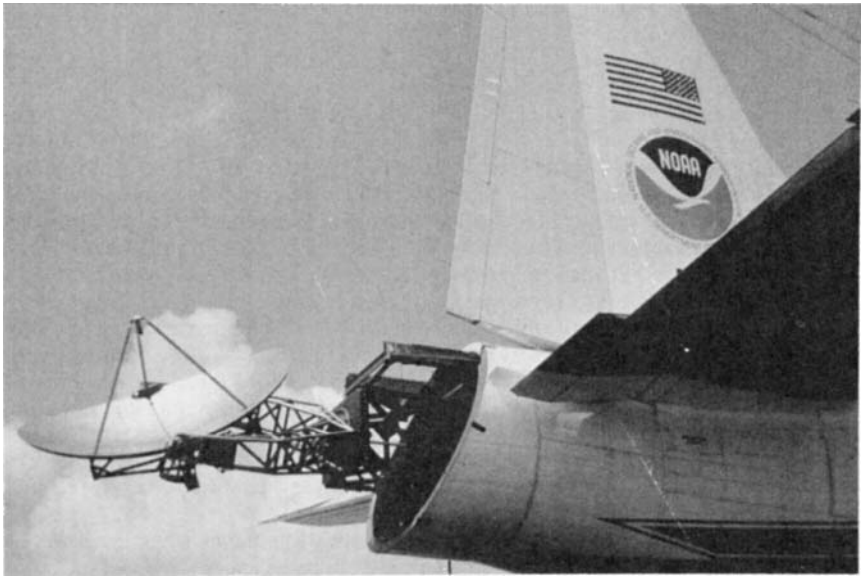

FIG. 23.9 Tail-mounted doppler radar antenna on the P-3 research and reconnaissance aircraft operated by the National Oceanic and Atmospheric Administration (NOAA).

can measure only two components of vector air motion, the assumption of mass continuity is invoked. The equation of continuity ($\nabla \cdot \overline{V} = 0$) is used to obtain the third-dimensional component, where $\overline{V}$ is the vector air motion. The vertical air motion is calculated from vertical integration of the continuity equation.

Walther, Frush, and Hildebrand[78] describe a next-generation airborne doppler radar system that consists of two antennas mounted in the tail—one pointed forward from the orthogonal plane by an angle of the order of 30° and one pointed rearward, also by about 30°. With such a system, each antenna scans in a conical surface—one cone pointing forward, one rearward—thus permitting synthesis of a dual-doppler radar system along the aircraft track. Because the aircraft need not fly orthogonal tracks, the time required for measurements of cloud systems is dramatically reduced. Moreover, severe storms (which could otherwise not be penetrated along an orthogonal track) can be observed fully by an aircraft outside the regions of severe weather.

Among the more significant challenges facing researchers today is the need to make global measurements of precipitation. Understanding of the global climate requires that quantitative measurements of precipitation be made throughout the world, particularly in the tropics and over the oceans. Satellite observations appear to offer the only practical mechanism for obtaining these measurements. Meneghini and Atlas[79] describe a concept for a dual-wavelength radar for precipitation measurements from space.

Clear-Air Radars. Another form of doppler radar that has become popular in the research community is the so-called wind profiler. Wind profilers usually

take the form of VHF and UHF fixed-beam systems, pointing vertically and at angles approximately 15° from the zenith. Such radars[7] can make doppler measurements throughout the range of altitudes from a few hundred meters to 15 km above the surface, depending upon the wavelength selected and the power-aperture product available. Very powerful radars of this type are referred to as Mesosphere, Stratosphere, Troposphere (MST) radars because of their ability to make measurements throughout most of these atmospheric regions. Powerful MST radars are operated at many laboratories around the world. Major facilities are located at Kiruna, Sweden; the Massachusetts Institute of Technology in Cambridge, Massachusetts; Arecibo, Puerto Rico; Jicamarca, Peru; and at the University of Kyoto in Japan.

These clear-air radars receive energy backscattered from index-of-refraction inhomogeneities due to atmospheric turbulence. The antenna systems usually take the form of phased arrays. Transmitters are generally in the form of high-powered, fully coherent transmitting tubes. One exception is at the University of Kyoto, where the antenna-transmitter system consists of more than 400 radiating elements, each with its own solid-state transmitter. This approach allows for full electronic scanning of the beam. A network of 400-MHz wind profilers in the central United States is also expected to use solid-state transmitters, but electronic scanning will not be possible.

The meteorological community is excited about these devices because of their ability to measure winds continuously. This capability permits the observation of smaller-scale temporal and spatial wind-field features than can be obtained from the global 12-hourly rawindsonde (balloon) networks. These smaller-scale measurements are important for understanding local and regional weather and for effective forecasting on these scales.

It is important to recognize that two-beam systems can measure horizontal winds if the wind field is uniform and if vertical velocities are negligible. A three-beam system can measure all three velocity components if the wind is uniform. Four- and five-beam systems allow one to determine the quality of the measurements by detecting the presence of nonuniformity. Carbone, Strauch, and Heymsfield[80] and Strauch et al.[81] address the issue of wind measurement error in detail.

The reader is referred to the review paper by Röttger and Larsen[82] for a thorough treatment of wind-profiler technology.

Synthetic Aperture Radar and Pulse Compression. Metcalf and Holm[83] and Atlas and Moore[84] have considered the use of synthetic aperture radar (SAR) in order to obtain high-resolution measurements from mobile airborne or space-borne platforms. In general, both papers conclude that the cross-beam resolution possible is inherently limited by the decorrelation time of the targets due to their turbulent motion. Consequently, SAR offers little advantage over real aperture systems for meteorological applications from aircraft. However, space-borne systems can effectively use SAR because of the high speed of the orbiting spacecraft.

Pulse compression is not generally used for meteorological applications because peak power is not usually a limitation on system performance. Keeler and Frush,[77] however, point out that pulse compression can be of benefit in some rapid-scanning applications. In situations where signals are very weak (such as for MST applications), pulse compression is used to increase system sensitivity by increasing the average power of the system.

A note of caution is in order when considering pulse compression for meteorological radars. This relates to the matter of range sidelobes. Careful design is necessary to minimize these sidelobes, just as antenna sidelobes should be minimized, in order to mitigate the effects of interpretive errors caused by wide-dynamic-range distributed weather targets.

REFERENCES

1. Serafin, R. J.: New Nowcasting Opportunities Using Modern Meteorological Radar, *Proc. Mesoscale Analysis Forecast. Symp.*, pp. 35–41, European Space Agency, Paris, 1987.
2. McCarthy, J., J. Wilson, and T. T. Fujita: The Joint Airport Weather Studies (JAWS) Project, *Bull. Am. Meteorol. Soc.*, vol. 63, pp. 15–22, 1982.
3. Lhermitte, R. M.: Dual-Doppler Radar Observations of Convective Storm Circulations, *Preprints, 14th Conf. Radar Meteorol.*, pp. 139–144, American Meteorological Society, Boston, 1970.
4. Hildebrand, P., and C. Mueller: Evaluation of Meteorological Airborne Doppler Radar, Part I: Dual-Doppler Analyses of Air Motions, *J. Atmos. Ocean. Technol.*, vol. 2, pp. 362–380, 1985.
5. Mueller, C., and P. Hildebrand: Evaluation of Meteorological Airborne Doppler Radar, Part II: Triple-Doppler Analysis of Air Motions, *J. Atmos. Ocean. Technol.*, vol. 2, pp. 381–392, 1985.
6. Hall, M. (ed.): Special papers: Multiple Parameter Radar Measurements of Precipitation, *Radio Sci.*, vol. 19, 1984.
7. Strauch, R. G., D. A. Merritt, K. P. Moran, K. B. Earnshaw, and D. Van De Kamp: The Colorado Wind Profiling Network, *J. Atmos. Ocean. Technol.*, vol. 1, pp. 37–49, 1984.
8. Serafin, R. J., and R. Strauch: Meteorological Radar Signal Processing, in "Air Quality Meteorology and Atmospheric Ozone," American Society for Testing and Materials, Philadelphia, 1977, pp. 159–182.
9. Gray, G. R., R. J. Serafin, D. Atlas, R. E. Rinehart, and J. J. Boyajian: Real-Time Color Doppler Radar Display, *Bull. Am. Meteorol. Soc.*, vol. 56, pp. 580–588, 1975.
10. Battan, L. J.: "Radar Observation of the Atmosphere," University of Chicago Press, 1973.
11. Doviak, R. J., and D. S. Zrnić: "Doppler Radar and Weather Observations," Academic Press, Orlando, Fla., 1984.
12. Bean, B. R., E. J. Dutton, and B. D. Warner: Weather Effects on Radar, in Skolnik, M. (ed.): "Radar Handbook," McGraw-Hill Book Company, New York, 1970, pp. 24-1–24-40.
13. Mie, G.: Beiträge zur Optik trüber Medien, speziell kolloidaler Metallösungen [Contribution to the optics of suspended media, specifically colloidal metal suspensions], *Ann. Phys.*, vol. 25, pp. 377–445, 1908.
14. Probert-Jones, J. R.: The Radar Equation in Meteorology, *Q. J. R. Meteorol. Soc.*, vol. 88, pp. 485–495, 1962.
15. Metcalf, J. I.: Airborne Weather Radar and Severe Weather Penetration, *Preprints, 19th Conf. Radar Meteorol.*, pp. 125–129, American Meteorological Society, Boston, 1980.
16. Allen, R. H., D. W. Burgess, and R. J. Donaldson, Jr.: Severe 5-cm Radar Attenuation of the Wichita Falls Storm by Intervening Precipitation, *Preprints, 19th Conf. Radar Meteorol.*, pp. 87–89, American Meteorological Society, Boston, 1980.
17. Eccles, P. J., and D. Atlas: A Dual-Wavelength Radar Hail Detector, *J. Appl. Meteorol.*, vol. 12, pp. 847–854, 1973.

18. Donaldson, R. J., Jr.: The Measurement of Cloud Liquid-Water Content by Radar, *J. Meteorol.*, vol. 12, pp. 238–244, 1955.

19. Weickmann, H. K., and H. J. aufm Kampe: Physical Properties of Cumulus Clouds, *J. Meteorol.*, vol. 10, pp. 204–221, 1953.

20. Gunn, K. L. S., and T. W. R. East: The Microwave Properties of Precipitation Particles, *Q. J. R. Meteorol. Soc.*, vol. 80, pp. 522–545, 1954.

21. Ryde, J. W., and D. Ryde: "Attenuation of Centimeter Waves by Rain, Hail, Fog, and Clouds," General Electric Company, Wembley, England, 1945.

22. Bean, B. R., and R. Abbott: Oxygen and Water Vapor Absorption of Radio Waves in the Atmosphere, *Geofis. Pura Appl.*, vol. 37, pp. 127–144, 1957.

23. Ryde, J. W.: The Attenuation and Radar Echoes Produced at Centimetre Wavelengths by Various Meteorological Phenomena, in "Meteorological Factors in Radio Wave Propagation," Physical Society, London, 1946, pp. 169–188.

24. Laws, J. O., and D. A. Parsons: The Relationship of Raindrop Size to Intensity, *Trans. Am. Geophys. Union*, 24th Annual Meeting, pp. 452–460, 1943.

25. Schelleng, J. C., C. R. Burrows, and E. B. Ferrell: Ultra-Short-Wave Propagation, *Proc. IRE*, vol. 21, pp. 427–463, 1933.

26. Medhurst, R. G.: Rainfall Attenuation of Centimeter Waves: Comparison of Theory and Measurement, *IEEE Trans.*, vol. AP-13, pp. 550–564, 1965.

27. Burrows, C. R., and S. S. Attwood: "Radio Wave Propagation, Consolidated Summary Technical Report of the Committee on Propagation, NDRC," Academic Press, New York, 1949, p. 219.

28. Humphreys, W. J.: "Physics of the Air," McGraw-Hill Book Company, New York, 1940, p. 82.

29. Atlas, D., and E. Kessler III: A Model Atmosphere for Widespread Precipitation, *Aeronaut. Eng. Rev.*, vol. 16, pp. 69–75, 1957.

30. Dennis, A. S.: Rainfall Determinations by Meteorological Satellite Radar, *Stanford Research Institute, SRI Rept.* 4080, 1963.

31. Kerker, M., M. P. Langleben, and K. L. S. Gunn: Scattering of Microwaves by a Melting Spherical Ice Particle, *J. Meteorol.*, vol. 8, p. 424, 1951.

32. "Glossary of Meteorology," vol. 3, American Meteorological Society, Boston, 1959, p. 613.

33. Best, A. C.: "Physics in Meteorology," Sir Isaac Pitman & Sons, Ltd., London, 1957.

34. Saxton, J. A., and H. G. Hopkins: Some Adverse Influences of Meteorological Factors on Marine Navigational Radar, *Proc. IEE (London)*, vol. 98, pt. III, p. 26, 1951.

35. Pasqualucci, F., B. W. Bartram, R. A. Kropfli, and W. R. Moninger: A Millimeter-Wavelength Dual-Polarization Doppler Radar for Cloud and Precipitation Studies, *J. Clim. Appl. Meteorol.*, vol. 22, pp. 758–765, 1983.

36. Lhermitte, R.: A 94-GHz Doppler Radar for Cloud Observations, *J. Atmos. Ocean. Technol.*, vol. 4, pp. 36–48, 1987.

37. Richter, J. H.: High-Resolution Tropospheric Radar Sounding, *Proc. Colloq. Spectra Meteorol. Variables, Radio Sci.*, vol. 4, pp. 1261–1268, 1969.

38. Tang Dazhang, S. G. Geotis, R. E. Passarelli, Jr., A. L. Hansen, and C. L. Frush: Evaluation of an Alternating PRF Method for Extending the Range of Unambiguous Doppler Velocity, *Preprints, 22d Conf. Radar Meteorol.*, pp. 523–527, American Meteorological Society, Boston, 1984.

39. Laird, B. G.: On Ambiguity Resolution by Random Phase Processing, *Preprints, 20th Conf. Radar Meteorol.*, p. 327, American Meteorological Society, Boston, 1981.

40. Rummler, W. D.: Introduction of a New Estimator for Velocity Spectral Parameters, *Tech. Memo. MM*-68-4121-5, Bell Telephone Laboratories, Whippany, N.J., 1968.

41. Hildebrand, P. H., and R. H. Sekhon: Objective Determination of the Noise Level in Doppler Spectra. *J. Appl. Meteorol.*, vol. 13, pp. 808–811, 1974.

42. Denenberg, J. N., R. J. Serafin, and L. C. Peach: Uncertainties in Coherent Measurement of the Mean Frequency and Variance of the Doppler Spectrum from Meteorological Echoes, *Preprints, 15th Conf. Radar Meteorol.*, pp. 216–221, American Meteorological Society, Boston, 1972.

43. Davenport, W. B., Jr., and W. L. Root: "An Introduction to the Theory of Random Signals and Noise," McGraw-Hill Publishing Company, New York, 1958.

44. Zrnić, D. S.: Estimation of Spectral Moments for Weather Echoes, *IEEE Trans.*, vol. GE-17, pp. 113–128, 1979.

45. Marshall, J. S., and W. Hitschfeld: The Interpretation of the Fluctuating Echo for Randomly Distributed Scatterers, pt. I, *Can. J. Phys.*, vol. 31, pp. 962–994, 1953.

46. Frush, C.: Doppler Signal Processing Using IF Limiting, *Preprints, 20th Conf. Radar Meteorol.*, pp. 332–337, American Meteorological Society, Boston, 1981.

47. Mueller, E. A., and E. J. Silha: Unique Features of the CHILL Radar System, *Preprints, 18th Conf. Radar Meteorol.*, pp. 381–386, American Meteorological Society, Boston, 1978.

48. Campbell, S. D., and S. H. Olson: Recognizing Low-Altitude Wind Shear Hazards from Doppler Weather Radar: An Artificial Intelligence Approach, *J. Atmos. Ocean. Technol.*, vol. 4, p. 518, 1987.

49. Baynton, H. W., R. J. Serafin, C. L. Frush, G. R. Gray, P. V. Hobbs, R. A. Houze, Jr., and J. D. Locatelli: Real-Time Wind Measurement in Extratropical Cyclones by Means of Doppler Radar, *J. Appl. Meteorol.*, vol. 16, pp. 1022–1028, 1977.

50. Wilson, J., and H. P. Roesli: Use of Doppler Radar and Radar Networks in Mesoscale Analysis and Forecasting, *ESA J.*, vol. 9, pp. 125–146, 1985.

51. Bonewitz, J. D.: The NEXRAD Program—An Overview, *Preprints, 20th Conf. Radar Meteorol.*, pp. 757–761, American Meteorological Society, Boston, 1981.

52. Gunn, R., and Kinzer, G. D.: The Terminal Velocity of Fall for Water Droplets in Stagnant Air, *J. Meteorol.*, vol. 6, pp. 243–248, 1949.

53. Marshall, J. S., and W. M. K. Palmer: The Distribution of Raindrops with Size, *J. Meteorol.*, vol. 4, pp. 186–192, 1948.

54. Blanchard, D. C.: Raindrop Size Distribution in Hawaiian Rains, *J. Meteorol.*, vol. 10, pp. 457–473, 1953.

55. Jones, D. M. A.: 3 cm and 10 cm Wavelength Radiation Backscatter from Rain, *Proc. Fifth Weather Radar Conf.*, pp. 281–285, American Meteorological Society, Boston, 1955.

56. Gunn, K. L. S., and J. S. Marshall: The Distribution with Size of Aggregate Snowflakes, *J. Meteorol.*, vol. 15, pp. 452–466, 1958.

57. Wilson, J. W., and E. A. Brandes: Radar Measurement of Rainfall—A Summary, *Bull. Am. Meteorol. Soc.*, vol. 60, pp. 1048–1058, 1979.

58. Bridges, J., and J. Feldman: An Attenuation Reflectivity Technique to Determine the Drop Size Distribution of Water Clouds and Rain, *J. Appl. Meteorol.*, vol. 5, pp. 349–357, 1966.

59. Seliga, T. A., and V. N. Bringi: Potential Use of Radar Differential Reflectivity Measurements at Orthogonal Polarizations for Measuring Precipitation, *J. Appl. Meteorol.*, vol. 15, pp. 69–76, 1976.

60. Zawadzki, I.: Factors Affecting the Precision of Radar Measurements of Rain, *Preprints, 22d Conf. Radar Meteorol.*, pp. 251–256, American Meteorological Society, Boston, 1984.

61. Burgess, D., et al.: Final Report on the Joint Doppler Operational Project (JDOP), 1976–1978, *NOAA Tech. Memo. ERL NSSL-86*, 1979.

62. Armstrong, G. M., and R. J. Donaldson, Jr.: Plan Shear Indicator for Real-Time Doppler Identification of Hazardous Storm Winds, *J. Appl. Meteorol.*, vol. 8, pp. 376–383, 1969.

63. Donaldson, R. J., Jr.: Vortex Signature Recognition by a Doppler Radar, *J. Appl. Meteorol.*, vol. 9, pp. 661–670, 1970.

64. Zrnić, D. S., and R. J. Doviak: Velocity Spectra of Vortices Scanned with a Pulse Doppler Radar, *J. Appl. Meteorol.*, vol. 14, pp. 1531–1539, 1975.

65. Fujita, T., and F. Caracena: An Analysis of Three Weather-Related Aircraft Accidents, *Bull. Am. Meteorol. Soc.*, vol. 58, pp. 1164–1181, 1977.

66. Fujita, T.: "The Downburst," Satellite and Mesometeorology Research Project, Department of the Geophysical Sciences, University of Chicago, 1985.

67. Fujita, T.: "The DFW Microburst," Satellite and Meteorology Research Project, Department of the Geophysical Sciences, University of Chicago, 1986.

68. McCarthy, J., and R. Serafin: The Microburst: Hazard to Aviation, *Weatherwise*, vol. 37, no. 3, pp. 120–127, 1984.

69. McCarthy, J., J. Wilson, and M. Hjelmfelt: Operational Wind Shear Detection and Warning: The CLAWS Experience at Denver and Future Objectives, *Preprints, 23d Conf. Radar Meteorol.*, pp. 22–26, American Meteorological Society, Boston, 1986.

70. Witt, A., and S. P. Nelson: The Relationship between Upper-Level Divergent Outflow Magnitude as Measured by Doppler Radar and Hailstorm Intensity, *Preprints, 22d Conf. Radar Meteorol.*, pp. 108–111, American Meteorological Society, Boston, 1984.

71. Aydin, K., T. A. Seliga, and V. Balaji: Remote Sensing of Hail with a Dual Linear Polarization Radar, *J. Clim. Appl. Meteorol.*, vol. 25, pp. 1475–1484, 1986.

72. Lhermitte, R. M., and D. Atlas: Precipitation Motion by Pulse Doppler Radar, *Proc. Ninth Weather Radar Conf.*, pp. 218–223, American Meteorological Society, Boston, 1961.

73. Browning, K. A., and R. Wexler: A Determination of Kinematic Properties of a Wind Field Using Doppler Radar, *J. Appl. Meteorol.*, vol. 7, pp. 105–113, 1968.

74. Wilson, J. W., and W. E. Schreiber: Initiation of Convective Storms at Radar-Observed Boundary Layer Convergence Lines, *Mon. Weather Rev.*, vol. 114, pp. 2516–2536, 1986.

75. Carbone, R. E.: A Severe Frontal Rainband, Part I: Storm-Wide Hydrodynamic Structure, *J. Atmos. Sci.*, vol. 39, pp. 258–279, 1982.

76. Brook, M., and P. Krehbiel: A Fast-Scanning Meteorological Radar, *Preprints, 16th Conf. Radar Meteorol.*, pp. 26–31, American Meteorological Society, Boston, 1975.

77. Keeler, R. J., and C. L. Frush: Rapid-Scan Doppler Radar Development Considerations, Part II: Technology Assessment, *Preprints, 21st Conf. Radar Meteorol.*, pp. 284–290, American Meteorological Society, Boston, 1983.

78. Walther, C., C. Frush, and P. Hildebrand: The NCAR Airborne Doppler Radar, Part III: Overview of Radar Design Details, *Preprints, 23d Conf. Radar Meteorol.*, vol. I, pp. 155–158, American Meteorological Society, Boston, 1986.

79. Meneghini, R., and D. Atlas: Simultaneous Ocean Cross-Section and Rainfall Measurements from Space with a Nadir-Looking Radar, *J. Atmos. Ocean. Technol.*, vol. 3, pp. 400–413, 1986.

80. Carbone, R. E., R. Strauch, and G. M. Heymsfield: Simulation of Wind Profilers in Disturbed Conditions, *Preprints, 23d Conf. Radar Meteorol.*, vol. I, pp. 44–47, American Meteorological Society, Boston, 1986.

81. Strauch, R. G., B. L. Weber, A. S. Frisch, C. G. Little, D. A. Merritt, K. P. Moran, and D. C. Welsh: The Precision and Relative Accuracy of Profiler Wind Measurements, *J. Atmos. Ocean. Technol.*, vol. 4, pp. 563–571, 1987.

82. Röttger, J., and M. F. Larsen: Clear Air Radar Techniques, invited paper, *40th Conf.*

Radar Meteorol., American Meteorological Society, Boston, 1987. Published in Atlas, D. (ed.): "Radar Meteorology," American Meteorological Society, Boston, 1989.

83. Metcalf, J. I., and W. A. Holm: Meteorological Applications of Synthetic Aperture Radar, final report, Project A-2101, Engineering Experiment Station, Georgia Institute of Technology, 1979.

84. Atlas, D., and R. K. Moore: The Measurement of Precipitation with Synthetic Aperture Radar, *J. Atmos. Ocean. Technol.*, vol. 4, pp. 368–376, 1987.